RSC Advances

This is an *Accepted Manuscript*, which has been through the Royal Society of Chemistry peer review process and has been accepted for publication.

Accepted Manuscripts are published online shortly after acceptance, before technical editing, formatting and proof reading. Using this free service, authors can make their results available to the community, in citable form, before we publish the edited article. This *Accepted Manuscript* will be replaced by the edited, formatted and paginated article as soon as this is available.

You can find more information about *Accepted Manuscripts* in the Information for Authors.

Please note that technical editing may introduce minor changes to the text and/or graphics, which may alter content. The journal's standard Terms & Conditions and the Ethical guidelines still apply. In no event shall the Royal Society of Chemistry be held responsible for any errors or omissions in this *Accepted Manuscript* or any consequences arising from the use of any information it contains.

ROYAL SOCIETY OF CHEMISTRY

www.rsc.org/advances

RSC Advances

Dynamic Article Links ►

Cite this: DOI: 10.1039/c0xx00000x

www.rsc.org/xxxxxx

PAPER

Low temperature plasma processing of nc-Si/a-SiN_x:H QDs thin films with high carrier mobility and preferred (220) crystal orientation: a promising material for third generation solar cells

Basudeb Sain and Debajyoti Das*

Received (in XXX, XXX) Xth XXXXXXXXX 20XX, Accepted Xth XXXXXXXXX 20XX
DOI: 10.1039/b000000x

In view of potential applications in third generation nc-Si solar cells, nanocrystalline silicon quantum dots (nc-Si QDs) embedded in amorphous hydrogenated silicon-nitride dielectric matrix (a-SiN_x:H), the nc-Si/a-SiN_x:H QDs thin films, are produced by single step low temperature plasma processing of silane (SiH_4) and ammonia (NH_4) diluted in H_2, using planar inductively coupled rf plasma-CVD. By decreasing the deposition temperature over 400–100°C, the undoped nc-Si/a-SiN_x:H QDs thin films of varying crystallinity (82–37%) are obtained with Si-ncs of average size ~5.7 – 1.3 nm and number density ~10^{11} – 10^{12} cm^{-2}, providing a significantly wide range of band gap and high optical absorption (>10^5 cm^{-1}) with associated very high electrical conductivity, σ_D ~5.6×10^{-3} – 2.7×10^{-7} S cm^{-1} along with high carrier concentration, n_e ~9×10^{13} – 1.8×10^{10} cm^{-3}, significantly high electron mobility, μ_e ~426–103 $cm^2V^{-1}s^{-1}$ and photosensitivity varying within ~1×10^1 – 3×10^3. At reduced temperature (100°C), although the crystalline volume fraction decreases, the overall crystallinity is mostly populated by the ultra-nanocrystalline component with dominant (220) crystallographic orientation which has favored electrical transport in stacked layered devices. High-density tiny nc-Si QDs induce in reasonably widening the band gap even at very low nitrogen content, while sufficiently high σ_d with improved photosensitivity, (σ_{Ph}/σ_d ~3×10^3) is a consequence of significantly high electron mobility attained by virtue of efficient defect passivation by the high atomic hydrogen density of the low-pressure ICP plasma that finally assists in obtaining a promising low temperature grown material for suitable applications in third generation tandem structure nc-Si solar cells.

Introduction

Further improvements in efficient photovoltaic conversion of solar energy is restricted by two major hurdles: (i) photons with energy smaller than the energy gap E_g are not absorbed in the base material and (ii) carriers excited by high-energy photons ($E_{ph} > E_g$) lose excess energy to phonons due to thermalization process. In view of proficiently controlling the bottleneck, present research on solar photovoltaics configures conceptually new third generation solar cells that involve tandem structures composed of two or more cells with different band gaps of the absorbing layer, accommodating the significant part of the solar spectrum. In this context the nc-Si quantum dots (QDs) embedded in different dielectric matrix is being considered as of excellent utility in the fabrication of third generation solar cells wherein nc-Si absorber layer, in particular, could provide better stability against light induced degradation.[1–9]

The amorphous hydrogenated silicon-nitride containing nanocrystalline silicon quantum dots (nc-Si/a-SiN_x:H) with tunable band gap, has been found to be very promising as a new material for construction of different layers in tandem structure solar cells.[1,10] The matrix silicon-nitride (a-SiN_x:H) is found to be superior compared to others e.g., silicon oxide (SiO_x) and carbide (SiC_x), etc. Silicon-nitride (SiN_x) is being introduced as a material of high dielectric constant, high strength over a wide temperature range, low tunneling barrier as well as outstanding chemical inertness.[11–13] Besides these, it has excellent inherent antireflection and surface passivation properties which are very important in solar cell performance.[14]

The structure of hydrogenated nanocrystalline silicon-nitride thin films can be described qualitatively as an ensemble of nanometer scale silicon crystallites (nc-Si) embedded in amorphous silicon-nitride (a-SiN_x:H) matrix. The increasing nitrogenation to the network helps increasing the optical gap; however, the electrical transport properties follow a trade-off relation with band gap widening. The complexity in electrical conduction arises due to its inhomogeneous structure, which consists of a mixture of different phases: crystalline nano grains, nanocrystalline columns, hydrogenated amorphous silicon-nitride (a-SiN_x:H), defects at the boundaries between different phases and voids.[1,15] One way to improve the electrical conductivity is by increasing carrier concentration via doping and the other way is to increase carrier mobility via reduction of defect concentration that can be achieved by the formation of

RSC Advances Accepted Manuscript

continuous and dense network using high density plasma. Increase of carrier mobility for plasma deposited silicon based thin films is a challenging task due to the presence of different kinds of defects like, unsaturated dangling bonds, voids, dislocation, etc., in the materials. Inductively couple plasma CVD (ICP-CVD) is a new technique providing higher density of the plasma at a lower pressure that is often advantageous for the growth of less defective and more crystalline films even at a faster rate.[16] Effective passivation of dangling bonds by atomic hydrogen is required for useful conduction and that also gives significant photosensitivity in amorphous dominated network. However, excess H atoms will lead to poor physical and electrical properties. In addition, crystalline grains with thermodynamically preferred <220> crystallographic orientation are conducive to carrier transport.[17,18] The increased (220) grains are also important for the enhancement of open circuit voltage and reduction of photo-carrier losses in solar cells. Band gap is an important factor, which essentially makes bridge between different layers; therefore tuning of band gap in a wide range is needed for successful application of the material in different layers of tandem structure solar cells. Band gap can be tuned either by controlling the stoichiometry of the matrix material (a-SiN_x:H) or by varying the dot size comparable to Bohr radius of silicon due to quantum confinement effect[19] and the combination of these two induce widening the band gap significantly. Optical absorption is another important factor that determines the application of a material in intrinsic layer of solar cells. The material with higher optical absorption is better for achieving higher conversion efficiency for efficient utilization of the material in device application.

The present investigation deals with a comprehensive analysis of different physical properties including the electrical transport of undoped nc-Si/a-SiN_x:H QDs thin films of very high mobility, as a new kind of material grown by single step low temperature plasma processing using inductively coupled plasma-CVD. Various spectroscopic and microscopic characterizations have been performed in order to establish a correlation among the structural, morphological, compositional, optical, and electrical properties of the highly optimized silicon–nitrogen–hydrogen complex network for obtaining a promising material for applications in third generation tandem structure nc-Si solar cells.

Experimental section

Planar inductively coupled rf (13.56 MHz) plasma-CVD was employed to prepare thin films of nanocrystalline silicon quantum dots embedded in amorphous silicon-nitride matrix (nc-Si/a-SiN_x:H) on p-type (100) single crystal silicon wafers, Corning® Eagle2000™ glasses and carbon coated copper microscope grids. Silane (SiH_4) and ammonia (NH_3) with individual flow rates of 2.0 and 0.7 sccm, respectively, diluted in hydrogen (H_2) were used to create a low-pressure plasma at 30 mTorr. The growth (substrate) temperature was varied from 400 to 100°C. No post-deposition treatment e.g., thermal annealing was employed after growing the films. Thickness of the films was determined by a Dektak 6M stylus profiler. For uniform comparison, thickness of all the films was maintained at ~3000Å. The X-ray diffraction analysis was carried out using a conventional Cu K_α X-ray radiation (λ=1:5418Å) source and a Bragg diffraction set-up (Seifert 3000P). The Raman spectra were obtained by Renishaw inVia Micro-Raman spectrophotometer (Serial No. 12W143) at room temperature in a backscattering geometry, using 514 nm Ar^+ Laser as the excitation source, at a power density ~2 mW/cm^2. High-resolution transmission electron micrographs (HR-TEM) as well as selected-area electron diffraction (SAED) patterns were obtained on ~30 nm thick samples deposited on carbon coated copper microscope grids supplied by Pacific Grid-Tech, USA, using a JEOL-JSM2010 transmission electron microscope operating at 200 kV. The scanning transmission electron microscope (STEM) as well as energy dispersive X-ray (EDX) mapping was obtained using a UHR-FEG (JEOL 2100 TEM/STEM) transmission electron microscope operating at 200 kV. The silicon–hydrogen–nitrogen bonding structure of the films was investigated from the infrared vibrational spectra obtained by a Nicolet Magna-IR 750 FTIR spectrometer. The optical absorption and reflection measurements in the UV–visible region at room temperature were performed using a double beam spectrophotometer (Hitachi 330, Japan). Electrical conductivity of the samples was measured with coplanar Al electrodes deposited by thermal evaporation at room temperature, and the measurement was carried out in vacuum of $\sim10^{-6}$ Torr, using a Keithley 6517A electrometer, after annealing the samples at 375K for 1 h. The evacuation and the thermal annealing process were adopted to eliminate the effects of adsorbed gases and light induced degradation, if any. The carrier concentration and the Hall mobility were obtained from Hall-effect measurements, carried out at room temperature in a standard van der Pauw configuration by using an electromagnet with magnetic induction of 0.8 T.

Results and Discussion

Crystallographic orientation/texture

The results of X-ray measurements are given in Fig. 1 for the series of samples prepared at different growth temperature, T varying from 400 to 100°C with an interval of 50°C. The broad band centered at 2Θ~25° corresponds to the amorphous silicon component, whereas, the peaks at 2Θ=28.34°, 47.17° and 56.08° correspond to (111), (220) and (311) crystallographic planes of silicon, respectively. It has been identified that the diffraction intensity reduces monotonically with decreasing growth temperature, suggesting gradual deviation of crystallinity in the silicon network. The ratio of peak intensities, $Z_{(220)}$ [$=I_{(220)}/I_{(111)}$] and $Z_{(311)}$ [$=I_{(311)}/I_{(111)}$], have been used to monitor the evolution of the crystallographic texture as a function of T. The XRD peaks corresponding to (111) orientation are, in general, most intense, i.e., the silicon crystallites are preferentially grown along <111> crystallographic orientation. However, careful observation at the inset of Fig. 1 reveals that the relative intensity of the (220) peak, $Z_{(220)}$, gradually increases on decrease in T, when the network gradually shifts from a highly nanocrystalline structure towards (nc-Si)–to–(a-Si) transition region. The variation of $Z_{(311)}$, as shown in the same inset, is being observed to occur in an almost opposite fashion, gradually decreasing on reducing temperature. The <111> orientation arises from random nucleation whereas, <220> due to the growth of thermodynamically preferred grains.[20,21] The nanocrystalline network possess a marked (220)

RSC Advances Accepted Manuscript

 This journal is © The Royal Society of Chemistry [year]

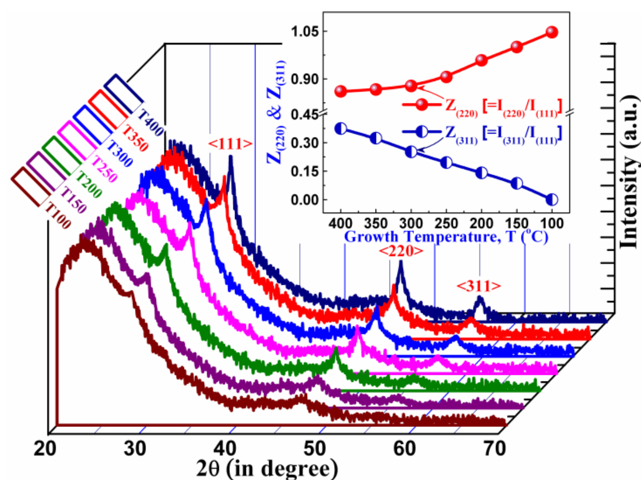

Fig. 1 X-ray diffraction spectra of nc-Si/a-SiN_x:H QDs thin films prepared at different growth temperature, *T*, varying from 400 to 100°C. Inset shows the variation of $Z_{(220)}$ [$=I_{(220)}/I_{(111)}$] and $Z_{(311)}$ [$=I(311)/I(111)$], with *T*.

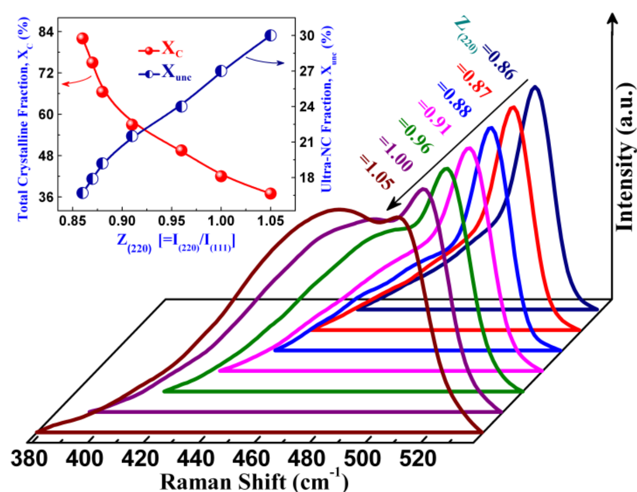

Fig. 2 First order Raman spectra for different $Z_{(220)}$. Red shift of the peak frequency has been directed by arrow. Inset presents the variations of total crystalline volume fraction (X_C) and ultra-nanocrystalline volume fraction (X_{unc}) with $Z_{(220)}$.

preferential growth at the transition towards amorphous structure at 100°C where <311> diffraction peak is virtually absent.

The average crystallite size of the silicon films has been estimated from the full width at half maximum (FWHM) of the (220) diffraction peaks using Debye-Scherrer formula and it has been found to reduce systematically from ~6 nm to 2.3 nm with the decrease of *T* from 400 to 100°C.

Two primary factors, growth temperature and gas dilution ratio mainly control the predominance of (220) oriented crystals in nc-Si:H.[22] A rise in the growth temperature favors (220) orientation, whereas, an increase in the hydrogen dilution ratio in the plasma increases the volume fraction of (111) grains compared to (220) grains. However, the present work that describes development of the nanocrystalline silicon-nitride thin films with a constant hydrogen dilution ~91.74%, shows increasing $Z_{(220)}$ at reduced growth temperatures, which appears to be an opposite nature of variation with growth temperature and at the same time an extremely useful phenomena concerning its device application. The evolution of this specific feature has been tried to be explained in the later section of this article.

Raman spectra: estimation of crystalline volume fraction and size of the nc-Si QDs

Raman spectra of the samples for different $Z_{(220)}$ have been displayed in Fig. 2. With increase of $Z_{(220)}$ from 0.86 to 1.05, a continuous red shift of peak frequency associated with asymmetric broadening in the line shape was identified, attributing modification in the nature of the network structure with simultaneous reduction in size of the crystalline grains. The above phenomena have been assigned as an effect due to the strong phonon confinement. Estimation of crystalline volume fraction from Raman spectra has been performed by deconvolution of each spectrum into three Gaussian components corresponding to nanocrystalline (nc-Si), amorphous (a-Si) and the intermediate ultra-nanocrystalline (unc-Si) component, described elsewhere.[21,23] The volume fractions of the individual components were estimated and the total crystalline volume fractions (X_C) were obtained as: $X_C = X_{nc} + X_{unc}$.[24] The estimated values of X_C and X_{unc} at different growth temperature (from 400 to 100°C), are given in Table I.

Table I Crystallinity and grain size of nc-Si/a-SiN_x:H QDs thin films prepared at different growth temperature, *T*.

Growth Temperature, *T* (°C)	Total Crystalline Volume Fraction, X_C (%)	Ultra-NC Volume Fraction, X_{unc} (%)	Grain Size (nm)
400	82	16.7	5.72
350	75	17.9	4.69
300	66.5	19.2	3.80
250	57	21.5	2.98
200	49.5	24	2.28
150	42	27	1.67
100	37	30	1.30

The reduction in overall crystallinity (corresponding to X_C varying from 82 to 37%) along with simultaneous increase in the ultra-nanocrystalline fraction, X_{unc}, from 16.7 to 30% during enhanced preferential growth along <220> crystallographic orientation, as shown at the inset in Fig. 2, identifies an interesting structural modification of the network with decreasing growth temperature from 400 to 100°C.

The present deposition condition promotes the low temperature grown crystallinity to be dominated by ultra-nanocrystalline component which are mostly <220> oriented. This favored ultra-nanocrystallinity with dominant <220> crystallographic orientation ($Z_{(220)}$=1.05) at the transition of nanocrystalline–to–amorphous (X_a ~63%) nitrogenated network structure obtained at low growth temperature (100°C), could be of significant advantage in electrical transportation when used in the devise structures. The present deposition condition promotes the low

RSC Advances Accepted Manuscript

Cite this: DOI: 10.1039/c0xx00000x

www.rsc.org/xxxxxx

PAPER

RSC Advances Accepted Manuscript

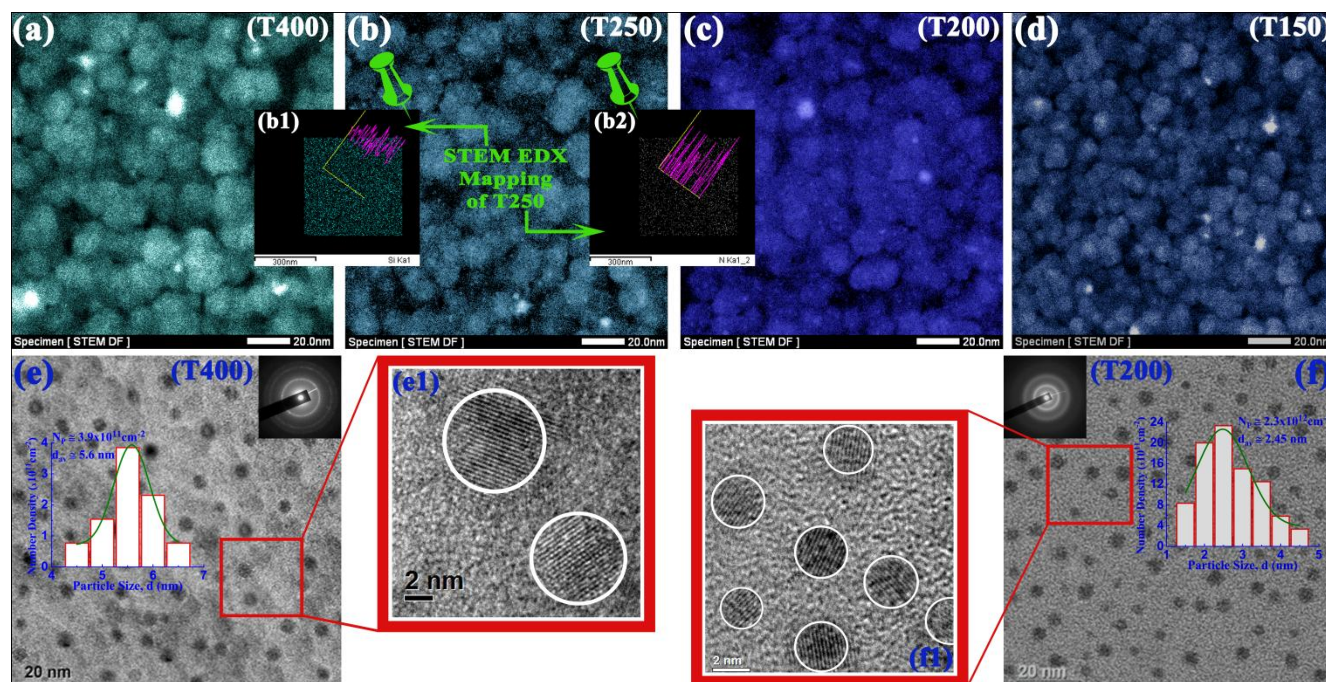

Fig. 4 (a)-(d) are the HAADF STEM images of the samples prepared at growth temperature, T = 400, 250, 200 and 150 °C. Insets (b1) & (b2) are the elemental maps obtained by integrating the Si K and N K EDX peak intensities, respectively, for sample prepared at T=250°C. (e),(e1) and (f),(f1) are the HR-TEM micrographs with low and high magnifications for the nc-Si/a-SiN_x:H QDs films prepared at T=400 and 200°C, respectively. Corresponding histograms demonstrate the distribution of number density with size of the Si nanocrystals, while the selected area diffraction pattern demonstrates the changes in the degree of crystallinity in each case.

temperature grown crystallinity to be dominated by ultra-nanocrystalline component which are mostly <220> oriented. This favored ultra-nanocrystallinity with dominant <220> crystallographic orientation ($Z_{(220)}$=1.05) at the transition of nanocrystalline–to–amorphous (X_a ~63%) nitrogenated network structure obtained at low growth temperature (100°C), could be of significant advantage in electrical transportation when used in the devise structures.

The average grain size has been estimated from Raman spectrum using the relation[24]

$$[\omega_L - \omega_0]^2 + \left(\frac{\Gamma_0}{2}\right)^2 \cong \frac{1}{3L} \cdot \exp(-\pi^2) \qquad (1)$$

where ω_L is the frequency of the crystalline like mode for a nanocrystal of size L. The ω_0 and Γ_0 are 520 and 3.5 cm^{-1}, respectively, for crystalline silicon. A continuous reduction in the size of the nanocrystals from ~5.72 nm at T=400°C to ~1.3 nm at T=100°C was obtained.

Z-Contrast HAADF STEM and HR-TEM analysis

Figs. 3(a)-(d) shows the HAADF STEM images of the samples prepared at growth temperature, T = 400, 250, 200 and 150 °C. In these images, darker contrast corresponds to regions that have a lower atomic number or density. Bright areas are related to higher atomic number or density which could be associated to Si-rich regions. The less bright areas (colored portion in individual image) relate the matrix region which includes hydrogenated amorphous silicon and silicon-nitride, whereas, the completely dark zones signify the presence of voids in the material. The Si-rich inclusions in the interface band do not percolate and their separation increases with lowering of growth temperature. The bulk part of the material is composed of clusters containing Si-rich regions, very few isolated grains, and little amount of voids in between the clusters. The space between the large clusters is filled up with different smaller clusters and grains, providing a good packing of the bulk network at the optimized parametric condition. The void fraction increases with decreasing growth temperature. Lowering of cluster size is being observed with the reduction of growth temperature. Figs. 3(b1) and 3(b2) are elemental maps obtained by integrating the Si K_α and N K_α EDX peak intensities, respectively, for sample prepared at T=250°C. From the EDX mappings, it is evident that Si and N are nearly homogeneously distributed in the composite structure. However, a careful observation reveals that there are several empty zones that appear in the N distribution and that support the existence of

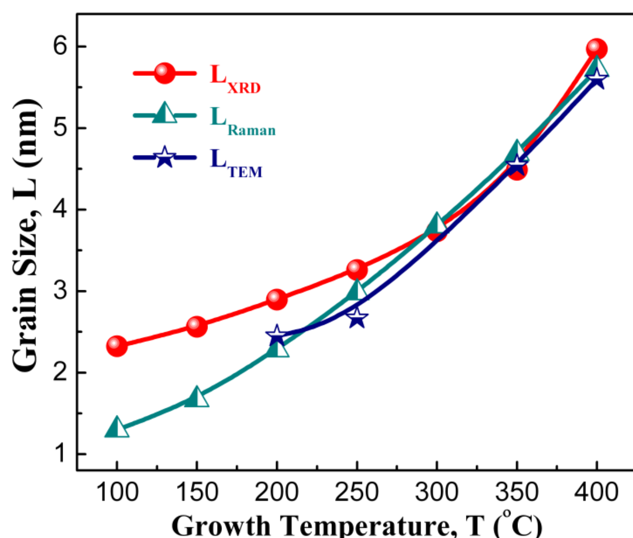

Fig. 4 Comparison on the nature of variation in the size of Si-ncs estimated from various spectroscopic and microscopic studies (XRD, Raman spectra and HR-TEM) with growth temperature, *T*.

Si-rich regions in the silicon-nitride network.

Details of internal microstructure were investigated using high-resolution TEM. The plan-view BF-HRTEM micrographs of the samples prepared at *T*=400 and 200°C have been displayed in Fig. 3(e) and 3(f), respectively. The sharp rings in the selected area electron diffraction (SAED) pattern (in inset of Fig. 3(e)) indicates that the material, T400 contains crystalline grains with three prominent orientations, <111>, <220> and <311>, having inter-planer spacing 0.312 nm, 0.198 nm and 0.162 nm, respectively. The SAED pattern for sample T200 (in inset of Fig. 3(f)), on the other hand, contains narrow diffuse rings, signifying that the material contains tiny crystallites with two prominent orientations, <111> and <220>. The presence of crystalline Si quantum dots of nano-dimension (nc-Si QDs) was obtained from HR-TEM imaging which are denser material and relatively dark in appearance, randomly distributed within less dense matrix (a-SiN_x:H). Fig. 3(e1) and 3(f1) represent the magnified view of the microstructure of samples T400 and T200, respectively. In both figures, the crystal planes are noticeable in all the marked areas identified as QDs, which are spherical in shape. The appearance of crystal planes in the magnified BF-HRTEM images and the rings in the SAED pattern confirms that the Si-rich regions in the HAADF-STEM images are the crystalline ones. A Gaussian like distribution of nanocrystals in each micrograph is presented by the corresponding histograms. The average size and number density of the nanocrystals have been identified from the corresponding peak of the distributions. The sample T400 possesses nc-Si QDs having an average size ~5.60 nm and density ~3.9×10^{11} cm^{-2}, while T200 contains nc-Si QDs of relatively small average size, ~2.45 nm but of higher density, ~2.3×10^{12} cm^{-2}. In addition, the HRTEM micrographs of the sample T350 and T250 (not being displayed here) contains nc-Si QDs having average size ~4.54 nm and 2.67 nm with density ~6.4×10^{11} and 1.12×10^{12} cm^{-2}, respectively. The monotonic reduction in average size of the QDs from 5.6 to 2.45 nm and the corresponding increase in the number density from ~3.9×10^{11} to 2.3×10^{-12} cm^{-1} with simultaneous broadening in the particle distribution are being observed, as growth temperature decreases from 400 to 200°C, before the network turned to mostly amorphous dominated (X_C=42%) at T=150°C.

Fig. 4 shows a fair comparison on various estimates of quantum dot size using different spectroscopic and microscopic tools and demonstrates miniaturization of nc-Si QDs with reduction of growth temperature. Size of the nanocrystals as estimated from the Raman spectra closely resembles to that calculated from HR-TEM micrographs. However, the size estimated from XRD spectra differs from the other estimations for temperatures below 250°C and the increasing difference at lower temperatures may be due to the limitation in the sensitivity of XRD estimation of nanocrystal size <2.5 nm.[25]

FTIR spectra: estimation of bonded nitrogen and hydrogen content

Fig. 5 shows the typical FTIR spectrum of the film with X_c= 49% prepared at *T*=200°C, where the characteristic features of silicon nitride, notably the Si–N symmetric and asymmetric stretching modes at ~480 and ~850 cm^{-1}, respectively, the Si–H stretching mode at ~2150 cm^{-1}, the Si–H wagging mode at 640 cm^{-1}, the N–H wagging/rocking mode at ~1170 cm^{-1} and the N–H stretching mode at ~3300 cm^{-1}, have been exhibited.[26,27] With the decrease of the growth temperature, the intensities of the all the Si–N, N–H and Si–H absorption peaks were observed to increase gradually, suggesting more and more nitrogen and hydrogen atoms are being incorporated into the films with lowering of the growth temperature. The bonded nitrogen content, *x* in SiN_x has been estimated from the Si–N asymmetric stretching mode vibration (~850 cm^{-1}), as

$$x = \frac{A_\omega}{N_{Si}} \int \frac{\alpha(\omega) d\omega}{\omega} \qquad (2)$$

where, the oscillator strength, A_ω=6.3×10^{18} cm^{-2} and N_{Si}=5×10^{22} cm^{-3} is the atomic density of crystalline silicon.[28] The nitrogen content increases monotonically with the decrease of growth temperature and the variation of which with *T* is shown in the inset of Fig. 5. At *T*= 400°C, the estimated *x* value is ~0.14, which increases rapidly with decreasing *T*, attains ~0.58 at *T*= 250°C and then gradually reaches to a value ~0.85 at *T*= 100°C.

The bonded hydrogen content C_H (in at %) has been estimated from the absorption peaks of the Si–H wagging mode at ~650 cm^{-1} and N–H stretching mode at ~3300 cm^{-1} using the following formula:

$$C_H = \left[\frac{A_\omega}{N_{Si}} \int \frac{\alpha(\omega) d\omega}{\omega} \right] \times 100\% \qquad (3)$$

where, A_ω=1.6×10^{19} cm^{-2} for Si-H wagging and 2.8×10^{20} cm^{-2} for N–H stretching, N_{Si}=5x $10^{22} cm^{-3}$.[29,30] The hydrogen content also increases monotonically similar to the variation of nitrogen content with the decrease of growth temperature, however, they follow a different nature of variation, as shown at the inset of Fig. 5. At *T* = 400°C, the estimated value of C_H is < 2 at% which gradually increases to a value ~5.8 at % at *T* = 250°C and than

RSC Advances Accepted Manuscript

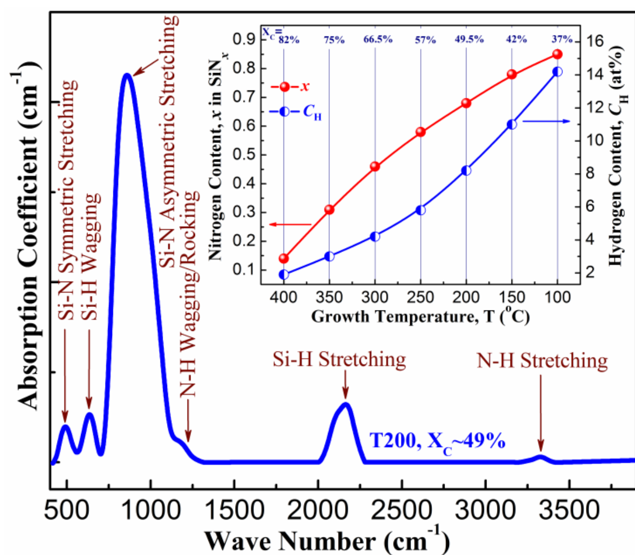

Fig. 5 Typical FTIR spectrum of the film with X_c= 49% prepared at T=200°C, where the characteristic features of silicon nitride, notably the Si–N symmetric and asymmetric stretching modes, the Si–H stretching and wagging modes and the N–H wagging/rocking and stretching modes, have been exhibited. Inset shows the variation of bonded nitrogen content, x in SiN_x and hydrogen content C_H (in at %), with T.

increases very rapidly to 14.2 at% at T = 100°C. The role of hydrogen in the network is to passivate dangling bonds which may be formed due to the binding of trivalent nitrogen atoms with the tetravalent silicon atoms in order to construct a continuous network. Dangling bonds may appear in the interface of silicon rich zones (silicon crystallites here) and in the a-SiN_x matrix. An effective passivation of those dangling bonds (nonradiative defect centers) helps electron-hole pairs to travel a long distance before recombination in the silicon-nitrogen-hydrogen network. The matrix phase is generally believed to be an amorphous network consisting of Si–Si, Si–N, Si–H and N–H bonds with bond energies of 1.83, 3.5, 3.0, and 4.0 eV, respectively, and the N–N bond is thought to be absent due to its lower energy (1.65eV) compared to the others.[31]

Optical Analysis

The optical density data of the samples prepared at different growth temperature was obtained from the absorbance and reflectance spectra of the films in the UV–visible region. The optical gap (E_g) was estimated from both the Tauc's[32] and Cody's[33] plot considering an indirect transition to take place within the material. Fig. 6 shows the variation of E_g with nitrogen content, x changing from 0.14 to 0.85, demonstrating a spontaneous enhancement of optical gap of the hetero-structure. The gradual widening of optical gap, E_g, (~2.26–2.65 eV from Tauc and ~1.73–2.25 eV from Cody) could be considered as an index of increasing both nitrogen content and hydrogen content in the silicon-nitrogen-hydrogen complex system having mostly crystalline network. In general, Tauc's gap shows higher values of band gap as compared to that obtained by Cody. But there is no clear physical principle to choose either model to estimate the optical band gap. In case of a mixed phase of crystalline,

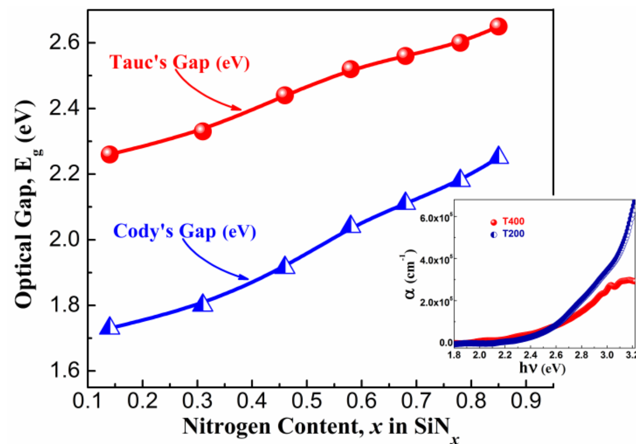

Fig. 6 Variation of optical gap, E_g, of nc-Si/a-SiN_x:H QDs thin films as a function of nitrogen content, x in SiN_x, estimated by using Tauc's[32] and Cody's[33] method. Inset shows the plot of optical absorption coefficient (α) versus photon energy (hν) for films deposited at T= 400 and 200°C.

amorphous and grain boundary, band gap should lie between amorphous and crystalline, depending upon the dominance of corresponding phases. However, for three-dimensionally confined Si nanocrystals in a-SiN_x:H matrix, both the Tauc's and Cody's gap may not give an appropriate assessment on the band gap of a mixed phase material showing quantum confinement effect, in principle, as it does not consider separately the contribution coming from individual effect, could only provide an average estimation that gives a logical variation.

The plot of optical absorption coefficient (α) versus photon energy (hν) of nc-Si/a-SiN_x:H QDs thin films deposited at T= 400 and 200°C is shown in the inset of Fig. 6, exhibiting high absorption (in the photon energy range from 2.25 to 3 eV) of the order of 10^5 cm^{-1}. The sample at T= 400°C demonstrates higher absorption at lower energies below 2.4 eV, whereas, above 2.4 eV the absorption is seen to be higher for T200 sample. The overall high absorption associated with excellent inherent antireflection property of silicon-nitride justifies its importance in solar cell.

Electrical conductivity, mobility and photosensitivity

Fig. 7(a) shows the variation of room temperature dark conductivity (σ_d), photoconductivity (σ_{ph}) and the photosensitivity (S_{ph}= σ_d/σ_{ph}) of the films, as a function of increasing nitrogen content, x in SiN_x. The nc-Si/a-SiN_x:H thin film at x = 0.14, possess dark conductivity, σ_d ~5.6x10^{-3} S cm^{-1} which is significantly high compared to the similar undoped silicon films reported in the literature.[15] The very high crystallinity ~82% of the present material could be one reason of having such a high conductivity.[34–36] The magnitude of dark conductivity decreases gradually with increasing nitrogen content at lower deposition temperature, reaches at ~1.0x10^{-3} S cm^{-1} at x = 0.46 and then decreases with relatively higher rate in attaining a value ~1.5x10^{-5} S cm^{-1} at x = 0.68, where the network structure contains crystallinity ~49%. On further increase of x, σ_d decreases further and that attains ~1.4x10^{-6} and ~2.7x10^{-7} S cm^{-1} at x =0.78 and 0.85, respectively. At T = 100°C, the network structure with x value 0.85, is mostly amorphous (X_a ~63%), containing ~30% of

This journal is © The Royal Society of Chemistry [year]
RSC Advances Accepted Manuscript

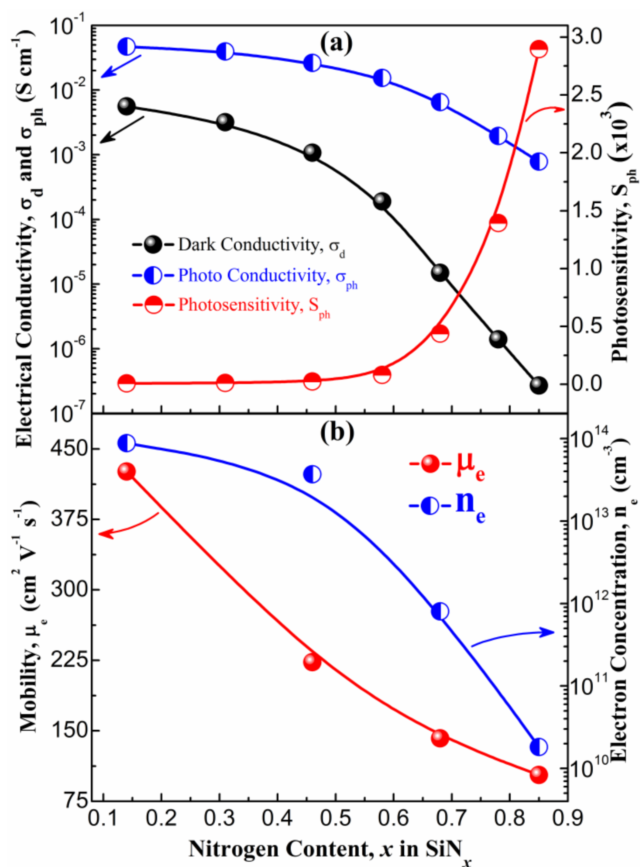

Fig. 7 (a) Variations in the room temperature dark conductivity (σ_D), photo conductivity (σ_{ph}) and the corresponding photosensitivity (S_{ph}) as a function of nitrogen content, x, for the nc-Si/a-SiN_x:H films prepared at decreasing T. (b) Variations of estimated electron mobility (μ_e) and carrier concentration (n_e) of the samples prepared at T=400, 300, 200, and 100°C, grown on crystalline silicon (c-Si) substrate, with increasing nitrogen content, x, in SiN_x.

ultra-nanocrystalline grains (X_{unc}) in overall crystalline volume fraction (X_C) of ~37 %. The photoconductivity, on the other hand, seems to reduce less sensitively, attaining σ_{ph} ~4.7x10^{-2} and ~7.8 x10^{-2} S cm^{-1} at x=0.14 and 0.85, respectively, leading to a large variation in photosensitivity, S_{ph} from ~10 to ~3x10^3, as shown in Fig. 7(a).

The mobility (μ_e) and carrier concentration (n_e) of the samples, grown on crystalline silicon (c-Si) substrates, were estimated from Hall-effect measurement at room temperature. The variation of estimated μ_e and n_e of four samples prepared at T=400, 300, 200, and 100°C with increasing nitrogen content, x in SiN_x, have been shown in Fig. 7(b). The Hall-effect data identifies the n-type electrical conduction of the undoped films. A very high electron mobility, μ_e = 426 cm^{2}V^{-1}s^{-1}, and high concentration of carrier electrons, n_e ~ 8.8x10^{13} cm^{-3}, have been estimated for the nc-Si/a-SiN_x:H film prepared at x=0.14. Both the mobility as well as electron concentration is grossly reduced to 223 cm^{2}V^{-1}s^{-1} and 3.7x10^{13} cm^{-3}, respectively, with the increase of nitrogen content to 0.46. At x=0.85, nc-Si/a-SiN_x:H network with an wide optical gap, E_g~ 2.65 eV (from Tauc's plot) along with corresponding μ_e ~103 cm^{2}V^{-1}s^{-1} and n_e ~ 1.8x10^{10} cm^{-3} has been attained.

The classical electron theory proposes that the electrical conductivity is determined by the free carrier concentration and the carrier mobility. The measured room temperature Hall mobility (μ_e) attached to the present work is quite high concerning different undoped crystalline/amorphous silicon/silicon-dielectric thin films, in general.[17,37–39] The highest value, 426 cm^{2}V^{-1}s^{-1}, is greater than the mobility earlier reported by us.[15] In fact, this will be the highest reported mobility compared to any plasma synthesized silicon based dielectric thin films containing silicon crystallites, as per our knowledge. The mobility strongly depends on charge carrier trap states and the potential energy barrier height at grain boundaries. In addition, the grain boundary defect density can be a deterministic factor of mobility in mixed phase materials like nc-Si/a-SiN_x:H QDs thin films. The highest mobility, 426 cm^{2}V^{-1}s^{-1}, obtained in this work may be attributed to the combined contribution from low charge carrier trap density, low defect density in the grain boundary, and very high crystallinity (~ 82%) that results an overall low grain boundary barrier potential. The low grain boundary defect density and charge carrier trap density may be the result of high surface coverage by atomic hydrogen, contributed from high density inductively coupled plasma associated with the proper optimization of the process parameters toward film deposition, and effective passivation of dangling bonds, as Si and N dangling bonds comprise a significant portion of the traps. The low grain boundary barrier potential could be explained by a grain boundary trapping model.[40] High X_C leads to the narrowing of the grain boundary barrier, as identified from HR-TEM images, shown in Fig. 3. Spontaneous reduction of mobility on increasing nitrogen content is attributed to the decreasing crystallinity and miniaturization of crystallite size that enhances the grain boundary barrier height. Besides these, there are further issues e.g., a particular material structure that could be accounted for high enough mobility (>100 cm^{2}V^{-1}s^{-1}) in the nc-Si/a-SiN_x:H film obtained even at a crystalline volume fraction as low as 37% at T= 100°C. Those are as follows; The crystallinity has been found to develop preferentially along the <220> orientation, showing gradually increasing $Z_{(220)}$ magnitude and simultaneously decreasing $Z_{(311)}$ magnitude in the XRD spectra (inset of Fig. 1). In particular, in the transition region where the network structure is mostly amorphous dominated, the crystal growth direction is dominated by <220>, which are reported to accelerate carrier transportation by increasing mobility in the nc-Si/a-SiN_x:H mixed-phase structure. The ultra-nanocrystalline component in the network significantly increases with x and those are mostly (220) dominated, as discussed earlier. The disordered gain-boundary regions around the ultra-nanocrystallites could provide a less defective amorphous network (with lower density of states) compared to the same around the large crystallites[15] which may also facilitate to maintain the electron mobility reasonably high even if in the amorphous dominated network structure.

The carrier concentration (n_e), another determining factor for conductivity, reduces grossly from 8.8x10^{13} to 1.8x10^{10} cm^{-3} due to increasing nitrogen content (from 0.14 to 0.85) in the Si-network. As for intrinsic nc-Si/a-SiN_x:H QDs thin films, n_e ~9x10^{13} cm^{-3} represents a very high carrier concentration; accordingly, the involvement of unforeseen impurities contributing to donors in the film causing unintentional doping of

RSC Advances Accepted Manuscript

the network might not be excluded from the involved growth process. Although the origin of the carriers in nc-Si/a-SiN_x:H has not been clarified, oxygen is, in general, an inherent residual incorporation in silicon based micro- and nano-structured films.[41] In case of nc-Si:H, in particular, oxygen located at grain boundaries is considered to act as n-type dopant.[34] The oxygen containing residuals (oxygen, water vapors, carbon oxides) adsorbed at the chamber wall may provide the dopant oxygen. In presence of nitrogenated precursors in abundance, oxygen incorporation in the network gets retarded which in turn could reduce the carrier concentration at higher nitrogen content. The very high mobility and high carrier concentration explain well the significantly high conductivity of the nc-Si/a-SiN_x:H QDs thin films in the present work.

The rising photosensitivity, S_{ph} of the nc-Si/a-SiN_x:H QDs thin films with increasing nitrogen content is mainly connected to the effective passivation of dangling bonds by atomic hydrogen. High dangling bond density in general reduces the mobility of photo-generated carriers, however, the mobility is being observed to be significantly high in the present films. High mobility facilitates the photo-generated carriers to travel a long distance without recombination, leading to significant photosensitivity in the material. In general, amorphous dominated films provide higher photosensitivity because of having lower density of states (DOS), as compared to crystalline films[42] and that explains very high photosensitivity (~$3x10^3$) from the sample with x= 0.85 in the transition region, which is mostly amorphous dominated (X_a~ 63%). Continuously increasing photosensitivity of the material with growing ultra-nanocrystalline component in the network at higher x, exhibiting S_{ph} ~$3x10^3$ at x=0.85, corresponding to hydrogen content, ~14.2 at %, insists on such an understanding. The nc-Si/a-SiN_x:H QDs thin films having significant conductivity and photosensitivity deserve enormous promise in view of its application as intrinsic layer in solar cells.

Plasma chemical reactions: Growth of nc-Si/a-SiN_x:H QDs thin films

In order to explain the formation processes of nc-Si/a-SiN_x:H QDs thin films by the inductively coupled plasma-CVD (ICP-CVD) at 13.56 MHz using the gas mixture of silane (SiH_4), ammonia (NH_3) and hydrogen (H_2), two separate reaction dynamics, gas-phase reaction and solid-phase reaction, are being considered. In the present deposition system the plasma is generated by a built in four-antenna low inductance flat spiral coil and the plasma is confined at the vicinity of the quartz plate of ICP source. ICP-discharges are produced by the rf power applied across a dielectric window via electromagnetic coupling advantageous for higher plasma density, lower plasma sheath potentials at the growth surface etc., compared to different other low-pressure plasma discharges. The growth holder is located at such a distance that the direct contact of the growth from the plasma could be avoided. Accordingly, the gas-phase transport of the precursors can be easily controlled by adjusting the gas pressure. Reactant gases are decomposed into various ions and radicals generated in the plasma. Depending on the reactivity and staying time in the plasma, etc., a selected fraction of those are able to take part in the film growth process.[43–45] Primarily, hydrogen atoms are produced in abundance by inductively coupled radio frequency (rf) discharge of H_2 mixed with ammonia (NH_3) and silane (SiH_4) in the plasma chamber.[46] Silyl (SiH_3), and amidogen (NH_2) radicals are produced from silane (SiH_4) and ammonia (NH_3) by atomic hydrogen induced gas phase reactions.[47] The NH_2 radicals are nonreactive with SiH_4, however, readily insert into SiH_3 and eliminate hydrogen, forming amino-silane complexes. Successive insertions of NH_2 into the complex continues to add amino groups and eliminate H, until reaching $Si(NH_2)_3$ and $Si(NH_2)_4$.[48,49] Different heterogeneous reactions of higher silanes, ammonia and the aminosilanes are considered to be the possible way for film growth.

In the next stage of growth three main models may be considered: a surface diffusion model, an etching model, and a chemical-annealing model. The structural network is primarily formed by the energy relaxation process of the adsorbed precursors on the growing surface and is principally determined by their surface diffusion length.[45,50] In contrast to the conventional capacitively coupled system, inductively coupled reactor (ICP) provides higher density of the plasma, which is often advantageous for the growth of less defective and more crystalline films that are important requirements in device application.[51] The high crystallinity (82 to 37%, as nitrogen content goes from 0.14 to 0.85) is the unique feature of high-density inductively coupled plasma, in which the high dissociation of SiH_4 and NH_3, even without H_2 dilution, provides very high surface coverage by large amount of atomic hydrogen flux produced by high density of electrons, n_0~10^{12} cm^{-3} at 10 mTorr, available in the low pressure inductively coupled plasma operating in the electromagnetic mode.[12] This high surface coverage by atomic hydrogen increases surface diffusion length of the radicals by lowering the surface diffusion activation energy. The large surface diffusion length facilitates the adsorbed radicals to reach the energetically convenient positions on the growing surface and that enables the formation of controlled hydrogenated nanocrystalline silicon-nitride film in nc-Si/a-SiN_x:H QDs configuration, even at 100°C growth temperature that contains a dot density ~10^{-12} cm^{-2} with 37% crystalline volume fraction. The high atomic hydrogen density present in the ICP plasma enhances the surface diffusion of SiH_x and NH_x radicals and the preferential etching of the loose and strained bonds induces rigid network structure. The sufficient local heating through hydrogen recombination on the growth surface that provides a continuous reordering of atomic elements, helps to form a network with better stability at minimum energy configuration, effective for device fabrication.

The size of silicon crystallites and film stoichiometry depend sensitively on the optimization of the process parameters which include chamber pressure, growth temperature, plasma power and gas flow rates, etc. All the films are deposited by ICP-CVD at very low flow rates of SiH_4 and NH_3, at low pressure in mTorr range, and at low growth temperature (400-100°C) with the intention of growing less defective network. However, the power delivered in the plasma was relatively high (500 W), providing higher energy to the precursors so as to maintain better kinetics on the growing surface. This amount of power is safely applied to our plasma chamber without any rupture of the film surface, as substrates are kept away from the plasma, separated by a metal grid, that maintains a remote-plasma like environment, favorable

RSC Advances Accepted Manuscript

This journal is © The Royal Society of Chemistry [year]

for growing less defective and high density silicon network that highly influences the carrier mobility and ultimate device performance.[52]

The undoped nc-Si/a-SiN_x:H QDs thin films with reasonably high electrical conductivity (5.6x10^{-3}-2.7x10^{-7} S cm^{-1}), carrier mobility (426-103 $cm^2V^{-1}s^{-1}$) and optical absorption (>10^5 cm^{-1}), obtained in the present work, deserve a high promise as a material suitable for nanocrystalline silicon solar cells. The films with wide variation in the crystallinity (82–37 %) and energy gap provide a significant photosensitivity (>10^3) at σ_D~ 10^{-6}-10^{-7} S cm^{-1}, with dominant (220) texture and ultra-nanocrystallie volume fraction in the transition region at lower temperatures (< 150°C). The development of nc-Si/a-SiN_x:H QDs thin films at constant hydrogen dilution ~91.74% is associated with increased $Z_{(220)}$ (=$I_{(220)}/I_{(111)}$) at reduced growth temperature. The opposite nature of variation of $Z_{(220)}$ with growth temperature, is significant. The dominated growth along <220> direction at lower growth temperature in the transition region, where the network structure becomes mostly amorphous dominated, could be beneficial for electrical transportation in the device. The increased (220) grains are important for the enhancement of open circuit voltage and reduction of photo-carrier losses in solar cells. The (220) nucleation of Si being the thermodynamically preferred orientation, corresponds to lower Gibbs free energy.[53] Microscopic observations identified fairly spherical shape with reduced corners and edges for the lower temperature grown Si QDs with smaller size having minimum surface area that involves lower Gibbs free energy and thus contributing (220) crystallographic orientation of the nanocrystals.[54]

A continuous red shift of the peak frequency and the broadening of first order Raman band have been identified, which has been associated to the strong phonon confinement. The confinement model using Gaussian function explains well the determination of the size of silicon nanocrystals from Raman shift, which varies between ~5.7-1.3 nm, supported well by XRD and HRTEM. The deposited films are associated with overall low hydrogen content, varying between ~1.9-14.2 at % with the lowering of growth temperature from 400-100°C, which is smaller compared to the nc-Si films deposited by glow discharge plasma-CVD.[55,56] A very high hydrogen content in the films in turn leads to poor material performance (e.g., degradation upon light exposure, etc.) in solar cells and other applications. The hydrogen dilution was constant at ~91.74% for all the films, while, the only variable was the growth temperature. Cheng *et al.*[57] reported very low hydrogen contents (4.4-2.7 at %) in nc-Si:H films deposited by ICP-CVD with the variation of hydrogen dilution from 50% to 95.24% at 200°C growth temperature. Compared to their work our samples also contain low H-content as per as the matrix a-SiN_x:H is considered, where the incorporation of N atoms in basic silicon network creates additional defects compared to a-Si:H. Here, the increased nitrogen content is associated with improved hydrogen content and that provides a proper balance needed for the formation of less defective network containing a minimum number of unsaturated dangling bonds at each growth temperature. Therefore, the nc-Si/a-SiN_x:H QDs thin films prepared by ICP-assisted CVD, having overall high conductivity, carrier mobility, optical absorption, photosensitivity and wide variation of optical gap associated with excellent inherent antireflection and surface passivation properties of the silicon-nitride matrix are particularly suitable for fabrication of all-silicon tandem solar cells.

Conclusions

A comprehensive analysis of different physical properties associated to inductively coupled plasma assisted growth of thin films of nanocrystalline silicon quantum dots embedded in hydrogenated amorphous silicon nitride matrix (nc-Si/a-SiN_x:H) has been presented in this work. The materials have been prepared using ICP-CVD with 13.56 MHz radio frequency, by changing the growth temperature, T, from 400 to 100°C, while maintaining a constant flow of silane (SiH_4) and ammonia (NH_4) within H_2-diluted plasma.

The relative intensity of the (220) peak in XRD, $Z_{(220)}$, gradually increases and attains an equal strength to that of (111) peak on decrease in T to 150°C and on further decrease of T to 100°C $Z_{(220)}$ becomes > 1. A dominant (220) crystallographic orientation happens to take place as the network approaches the (nc-Si)–to–(a-Si) transition region at lower deposition temperature. A continuous red shift of the peak frequency and the broadening of first order Raman band have been associated to the strong phonon confinement. The confinement model using Gaussian function explains well the determination of the size of silicon nanocrystals from Raman shift, which varies between ~5.7-1.3 nm and has been supported well by XRD and HRTEM data. The overall crystallinity (X_C) of the material is quite high, ~82% at T=400°C, as estimated from Raman analysis and that systematically reduces to ~37% at T=100°C. However, the volume fraction (X_{unc}) due to ultra nanocrystals and/or grain boundary component, which also contributes to the total amount of crystallinity, increases monotonically with decrease of growth temperature. The opposite nature of changes of X_C and X_{unc} with decreasing T identifies a definite modification of the network wherein ultra-nanocrystalline component dominates the crystallinity within mostly amorphous nitrogenated network structure obtained at lower deposition temperature. The present deposition condition promotes the ultra-nanocrystalline component to be dominated by (220) crystallographic orientation, which could provide beneficial contribution to the electrical transport within the amorphous dominated network structure in device configuration.

The highly nanocrystalline material (nc-Si/a-SiN_x:H QDs) obtained at T=400°C, possess nitrogen content, x ~0.14, a very low hydrogen content ~1.8 at %, high optical absorption (>10^5 cm^{-1}), wide optical gap and an associated significantly high room temperature dark conductivity σ_d ~5.6x10^{-3} S cm^{-1}, with the advent of high carrier concentration, n_e ~9x10^{13} cm^{-3} and a very high electron mobility, μ_e ~426 $cm^2V^{-1}s^{-1}$. Gradual decrease of T systematically enhances the optical band gap, however, reduces σ_d by several orders of magnitude to ~10^{-7} S cm^{-1} at T=100°C, corresponding to a nitrogen content ~0.85 at%, hydrogen content ~14.2 at % and mobility ~103 $cm^2V^{-1}s^{-1}$. The photoconductivity, on the other hand, seems to reduce less sensitively, attaining σ_{ph} ~10^{-4} S cm^{-1} at T=100°C, leading to a significantly high photosensitivity, S_{ph} ~3x10^3, as a consequence of effective passivation of dangling bonds by atomic hydrogen. In addition to the effect of reduced crystallinity and grossly diminishing carrier

RSC Advances Accepted Manuscript

concentration, the lowering in room temperature dark conductivity on increasing nitrogen content is a consequence of spontaneous reduction of mobility caused by the miniaturization of nanocrystallite size which eventually enhances the grain boundary barrier height.

The present undoped nc-Si/a-SiN_x:H QDs thin films with dominant (220) crystallographic orientation of the nanocrystallites of average size ~5.7 – 1.3 nm and number density ~10^{11} – 10^{12} cm^{-2}, providing a significantly high optical absorption (>10^5 cm^{-1}) with associated very high electrical conductivity, σ_D ~$5.6x10^{-3}$ – $2.7x10^{-7}$ S cm^{-1} along with high carrier concentration, n_e ~$9x10^{13}$ – $1.8x10^{10}$ cm^{-3}, electron mobility, μ_e ~426–103 $cm^2V^{-1}s^{-1}$ and photosensitivity ~$1x10^1$-$3x10^3$, happens to possess enormous promise as a material suitable for the fabrication of third generation nanocrystalline silicon solar cells in tandem structure.

Acknowledgement

The work has been done under nano-silicon projects funded by the Department of Science and Technology (Nano-Mission Program) and the Council of Scientific and Industrial Research, Government of India. The HR-TEM studies have been performed using facilities of Unit on Nano-Science at IACS. One of the authors (B.S.) acknowledges the Council of Scientific and Industrial Research, Government of India, for providing him with a research fellowship (via Grant No. 09/080(0706)/2010-EMR-I) for the work.

Notes and references

Nano-Science Group, Energy Research Unit, Indian Association for the Cultivation of Science, Jadavpur, Kolkata – 700 032, India.
** E-mail: erdd@iacs.res.in; Fax:+91(33)24732805.*

1 G. Conibeer, M. Green, E. C. Cho, D. König, Y. H. Cho, T. Fangsuwannarak, G. Scardera, E. Pink, Y. Huang, T. Puzzer, S. Huang, D. Song, C. Flynn, S. Park, X. Hao and D. Mansfield, *Thin Solid Films*, 2008, **516**, 6748.
2 L. Dal Negro, J. H. Yi, J. Michel, L. C. Kimerling, S. Hamel, A. Williamson and G. Galli, *IEEE J. Quantum Electron.*, 2006, **12**, 1628.
3 K. Ostrikov, *Rev. Mod. Phys.*, 2006, **77**, 489.
4 Y. H. So, S. Huang, G. Conibeer and M. A. Green, *EPL*, 2011, **96**, 17011.
5 J. Baxter, Z. Bian, G. Chen, D. Danielson, M. S. Dresselhaus, A. G. Fedorov, T. S. Fisher, C. W. Jones, E. Maginn, U. Kortshagen, A. Manthiram, A. Nozik, D. R. Rolison, T. Sands, L. Shi, D. Sholl and Y. Wu, *Energy Environ. Sci.*, 2012, **5**, 6040.
6 D. Das and A. Samanta, *Nanotechnology*, 2011, **22**, 055601.
7 K. S. Cho, N. M. Park, T. Y. Kim, K. H. Kim, G. Y. Sung and J. H. Shin, *Appl. Phys. Lett.*, 2005, **86**, 071909.
8 A. K. Panchal, D. K. Rai, M. Mathew and C. S. Solanki, *Nano*, 2009, **04**, 265.
9 D. Kar and D. Das, *J. Mater. Chem. A*, 2013, **1**, 14744.
10 E. C. Cho, M. A. Green, G. Conibeer, D. Song, Y. H. Cho, G. Scardera, S. Huang, S. Park, X. J. Hao, Y. Huang and L. Van Dao., *Adv. Optoelectron.*, 2007, **2007**, 69578.
11 M. Xu, S. Xu, J. W. Chai, J. D. Long and Y. C. Ee, *Appl. Phys. Lett.*, 2006, **89**, 251904.
12 Q. J. Cheng, S. Xu and K. Ostrikov, *J. Mater. Chem.*, 2010, **20**, 5853.
13 G. Y. Sung, N. M. Park, J. H. Shin, K. H. Kim, T. Y. Kim, K. S. Cho and C. Huh, *IEEE J. Quantum Electron.*, 2006, **12**, 1545.
14 H. K. Raut, V. A. Ganesh, A. S. Nairb and S. Ramakrishna, *Energy Environ. Sci.*, 2011, **4**, 3779.
15 D. Das and B. Sain, *J. Appl. Phys.*, 2013, **114**, 073708.
16 Q. J. Cheng, S. Xu and K. Ostrikov, *Acta. Mater.* 2010, **58**, 560.
17 D. Stieler, V. L. Dalal, K. Muthukrishnan, M. Noack and E. Schares, *J. Appl. Phys.*, 2006, **100**, 036106.
18 T. Kamiya, K. Nakahata, A. Miida, C. M. Fortmann and I. Shimizu, *Thin Solid Films*, 1999, **337**, 18.
19 D. Das, *Solid State Commun.*, 1998, **108**, 983.
20 V. L. Dalal, K. Muthukrishnan, X. Niu, and D. Stieler, *J. Non-Cryst. Solids*, 2006, **352**, 892.
21 D. Raha and D. Das, *Sol. Energy Mater. and Sol. Cells*, 2011, **95**, 3181.
22 Y. Toyoshima, K. Arai and A. Matsuda, *J. Non-Cryst. Solids*, 1989, **114**, 819.
23 D. Das, *Thin Solid Films*, 2005, **476**, 237.
24 B. Sain and D. Das, *Sci. Adv. Mater.*, 2013, **5**, 188.
25 D. Riabinina, C. Durand, J. Margot, M. Chaker, G. A. Botton and F. Rosei, *Phys. Rev. B*, 2006, **74**, 075334.
26 G. Lucovsky, J. Yang, S. S. Chao, J. E. Tyler and W. Czubatyj, *Phys. Rev. B*, 1983, **28**, 3234.
27 D. V. Tsu, G. Lucovsky and M. J. Mantini, *Phys. Rev. B*, 1986, **33**, 7069.
28 S. Hasegawa, H. Anbutsu and Y. Kurat, *Phil. Mag. B*, 1989, **59**, 365.
29 W. A. Lanford and M. J. Rand, *J. Appl. Phys.*, 1978, **49**, 2473.
30 C. J. Fang, K. J. Gruntz, L. Ley, M. Cardona, F. J. Demond, G. Muller and S. Kalbitzer, *J. Non-Cryst. Solids*, 1980, **35–36**, 255.
31 K. Maeda and I. Umezu, *J. Appl. Phys.*, 1991, **70**, 2745.
32 J. Tauc, R. Grigorovici and A. Vancu, *Phys. Status Solidi*, 1966, **15**, 627.
33 G. D. Cody, B. G. Brooks and B. Abeles, *Sol. Energy Mater.*, 1982, **8**, 231.
34 S. Miyajima, A. Yamada and M. Konagai, *Jpn. J. Appl. Phys.*, 2007, **46**, 1415.
35 S. J. Konezny, M. N. Bussac and L. Zuppiroli, *Appl. Phys. Lett.*, 2008, **92**, 012107.
36 D. Raha and D. Das, *J. Phys. D: Appl. Phys.*, 2008, **41**, 085303.
37 C. H. Lee, A. Sazonov and A. Nathan, *Appl. Phys. Lett.*, 2005, **86**, 222106.
38 T. Sameshima, K. Saitoh, N. Aoyama, S. Higashi, M. Kondo and A. Matsuda, *Jpn. J. Appl. Phys.*, 1999, **38**, 1892.
39 N. Pinto, M. Ficcadenti, L. Morresi, R. Murri, G. Ambrosone and Coscia U., *J. Appl. Phys.*, 2004, **96**, 7306.
40 G. Y. Hu, R. F. O'Connell, Y. L. He and M. B. Yu, *J. Appl. Phys.*, 1995, **78**, 3945.
41 S. Veprek, Z. Iqbal, R. O. Kuhne, P. Capezzuo, F. A. Sarott and J. K. Gimzevski, *J. Phys. C: Solid State Phys.* 1983, **166**, 241.
42 W. Paul and D. A. Anderson, *Sol. Energy Mater.*, 1981, **5**, 229.
43 D. Das, *Phys. Rev. B*, 1995, **51**, 10729.
44 A. Matsuda, J. Non-Cryst. Solids, 1983, **59 & 60**, 767.
45 D. Das, *Solid State Phenom.*, 1995, **44-46**, 227.
46 W. Hack, P. Rouveirolles and H. G. Wagner, *J. Phys. Chem.*, 1986, **90**, 2505.
47 D. L. Smith, A. S. Alimonda, C. C. Chen, W. Jackson and B. Wacker, *Mat. Res. Soc. Symp. Proc.*, 1988, **118**, 107.
48 D. B. Beach and J. M. Jasinski, *J. Phys. Chem.*, 1990, **94**, 3019.
49 B. Sain and D. Das, *Phys. Chem. Chem. Phys.*, 2013, **15**, 3881.
50 D. Das and M. Jana, Sol. Energy Mater. and Sol. Cells, 2004, **81**, 169.
51 S. Xu, K. N. Ostrikov, Y. Li, E. L. Tsakadze and I. R. Jones, *Phys. Plasmas*, 2001, **8**, 2549.

RSC Advances Accepted Manuscript

This journal is © The Royal Society of Chemistry [year]

52 S. Y. Myong, O. Shevaleevskiy, K. S. Lim, S. Miyajima and M. Konagai, *J. Appl. Phys.*, 2005, **98**, 054311.
53 F. Zhang, Z. Zheng, Y. Chen, D. Liu and X. Liu, *J. Appl. Phys.*, 1998, **83**, 4101.
5 54 Q. Cheng, E. Tam, S. Xu and K. Ostrikov, *Nanoscale*, 2010, **2**, 594.
55 U. Kroll, J. Meier, A. Shah, S. Mikhailov and J. Weber, *J. Appl. Phys.*, 1996, **80**, 4971.
56 N. R. Mavilla, C. S. Solanki and J. Vasi, *IEEE J. Photovolt.*, 10 2013, **4**, 1279.
57 Q. Cheng, S. Xu and K. Ostrikov, *J. Mater. Chem.*, 2009, **19**, 5134.

RSC Advances Accepted Manuscript

Table of Contents

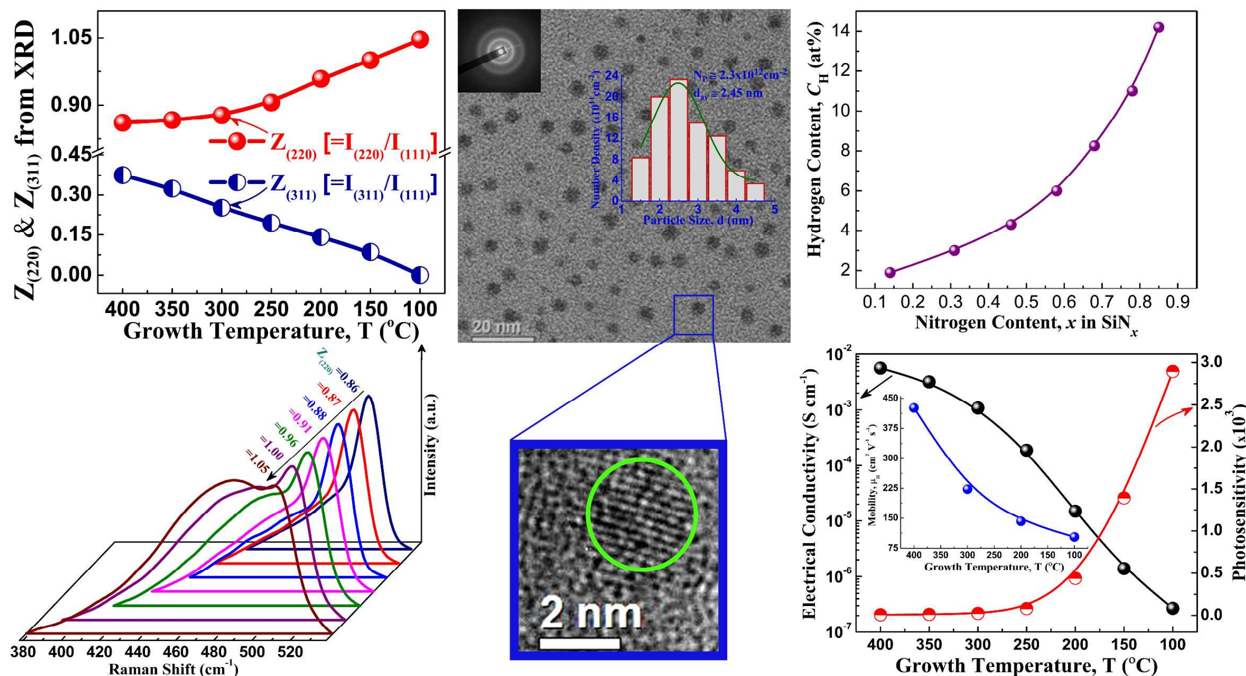

The nc-Si-QDs/a-SiN_x:H (~5.7–1.3 nm) thin-films grown by low-temperature Inductively-coupled plasma, possess high carrier-mobility, electrical-conductivity, photosensitivity and preferred (220) crystal orientation, suitable for third-generation solar cells.

RSC Advances Accepted Manuscript